Langmuir

Article

pubs.acs.org/Langmuir

Why Extreme Dilutions Reach Non-zero Asymptotes: A Nanoparticulate Hypothesis Based on Froth Flotation

Prashant S. Chikramane,[†] Dhrubajyoti Kalita,[†] Akkihebbal K. Suresh,[†,‡] Shantaram G. Kane,*[,†] and Jayesh R. Bellare*[,†,‡]

[†]Department of Chemical Engineering and [‡]Department of Biosciences and Bioengineering, Indian Institute of Technology (IIT) Bombay, Adi Shankaracharya Marg, Powai, Mumbai −400076, Maharashtra, India

Supporting Information

ABSTRACT: Extreme dilutions, especially homeopathic remedies of 30c, 200c, and higher potencies, are prepared by a process of serial dilution of 1:100 per step. As a result, dilution factors of 10^{60}, 10^{400}, or even greater are achieved. Therefore, both the presence of any active ingredient and the therapeutic efficacy of these medicines have been contentious because the existence of even traces of the starting raw materials in them is inconceivable. However, physicochemical studies of these solutions have unequivocally established the presence of the starting raw materials in nanoparticulate form even in these extreme (super-Avogadro, $>10^{23}$) dilutions. In this article, we propose and validate a hypothesis to explain how nanoparticles are retained even at such enormous dilution levels. We show that once the bulk concentration is below a threshold level of a few nanograms/milliliter (ng/mL), at the end of each dilution step, all of the nanoparticles levitate to the surface and are accommodated as a monolayer at the top. This dominant population at the air−liquid interface is preserved and carried to the subsequent step, thereby forming an asymptotic concentration. Thus, all dilutions are only apparent and not real in terms of the concentrations of the starting raw materials.

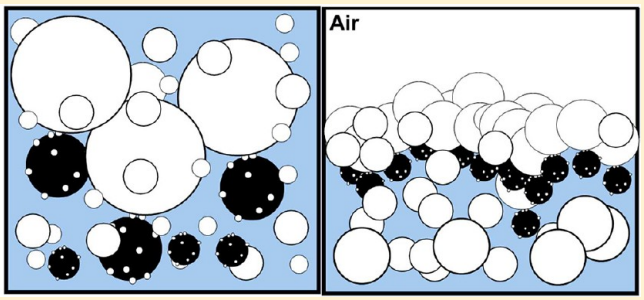

INTRODUCTION

This article is about extremely high dilutions of starting raw materials that arise in several industrial and biological applications. The process of manufacturing homeopathic medicines employs extreme dilutions even beyond what the atomistic theory of matter provides, leading to doubts regarding the existence of starting materials in these formulations. We show here that a finite amount of starting material remains in the finished product even at these extremely high dilutions. Our conclusions arise from our experiments indicating that in the successive dilution process of manufacturing, beyond a certain stage, the dilution is merely apparent and the concentration of the starting material in the diluted product reaches a non-zero asymptotic level no matter how much more the sample is diluted.

Homeopathy, since its inception in the late eighteenth century, has been used extensively for the treatment of various ailments while also being the epicenter of controversy. This therapy is based on the tenet that a solution of a particular substance (though highly toxic at high concentrations) when diluted several fold (on the order of 10^{60} or even greater), accompanied by a vigorous shaking process called succussion at every dilution step, imparts a potent activity with medicinal value. The scientific question often posed is, How are the homeopathic medicines active when they are used at extreme dilution, often well beyond Avogadro's number, wherein the presence of even remnants of the starting materials is unimaginable?

To answer the above question, several hypotheses invoking liquid memory,[1−4] clathrate formation,[5] and quantum physical[6,7] aspects have been put forth. However, insufficient validation and the speculative nature of these hypotheses have drawn severe criticism. Only the silica hypothesis[8] invokes the presence of physical entities. Recently, contrary to the existing beliefs that these dilutions would be devoid of any physical entities, Chikramane et al.[9] found that homeopathic medicines prepared using metal powders as the starting raw materials retained them even at extreme potencies of 30c and 200c (dilution factors of 10^{60} and 10^{400}, respectively), much beyond Avogadro's number. In spite of such enormous dilutions, nanoparticles of the metals ranging in sizes from 5 to 10 nm were detected by transmission electron microscopy (TEM) and electron diffraction (ED). Another significant observation was that the concentrations of these starting materials, albeit at extremely low (picogram/milliliter) levels, did not decrease as expected with serial dilutions but instead formed an asymptote beyond the 6c potency (dilution factor of 10^{12}).

In this article, we unravel the mystery of how particles are retained despite extreme dilutions. Using gold nanoparticles

Received: August 29, 2012
Revised: October 18, 2012

   dx.doi.org/10.1021/la303477s | *Langmuir* XXXX, XXX, XXX−XXX

(AuNP's), we performed controlled experiments closely mimicking the homeopathic manufacturing process of successive dilution with succussion and analyzed the concentration of gold in various parts of the sample. Our results suggest that the particles of the starting raw materials preferentially get adsorbed at the air−liquid interface, which is retained through the serial dilutions, thus attaining a nonzero asymptotic state. On the basis of the results that we obtained, we propose a hypothesis of particle retention that explains the presence of the starting material despite enormous dilutions, thereby resolving the homeopathic conundrum and reconciling it with the atomistic theory of matter.

EXPERIMENTAL SECTION

Materials. The chemicals used were procured from the following sources: Hydrogen tetrachloroaurate(III) trihydrate ($HAuCl_4{\cdot}3H_2O$) was obtained from Acros Organics, USA. Hydrochloric acid (HCl) AR, nitric acid (HNO_3) AR, sodium borohydride ($NaBH_4$) AR, sodium hydroxide (NaOH) AR, and potassium bromide (KBr) AR were obtained from Merck India Ltd. Lactose monohydrate AR and zinc (Zn) dust AR (~325 mesh particles) were obtained from SD Fine Chemicals Ltd. and Sisco Research Laboratories, India, respectively. The HPLC-grade ethanol was acquired from Commercial Alcohols Inc., Canada. The TEM grids obtained from Pacific Grid-Tech (USA) were 200 mesh copper grids coated with Formvar-Carbon.

Methods. *Synthesis of AuNP's.* We used synthetic AuNP's to mimic the ultrafine gold powder resulting from the grinding process in traditional homeopathic medicines. Approximately 40 mg of $HAuCl_4{\cdot}3H_2O$ was dissolved in 2 mL of a 50 mM solution of HCl to obtain the desired 50 mM solution. Similarly, an equimolar solution of $NaBH_4$ was prepared by dissolving approximately 38 mg in 20 mL of 50 mM NaOH solution. The $HAuCl_4{\cdot}3H_2O$ (1 mL) solution was slowly added to 100 mL of Milli-Q water with vigorous stirring at room temperature. $NaBH_4$ solution (6.5 mL) was slowly added, and the mixture was stirred for approximately 5 min until there was a distinct color change from light yellow to wine red.[10] The assembly was then placed in an oil bath maintained at 100 °C for 5 min. After the completion of the reaction, as monitored by UV−vis spectroscopic analyses, the reaction mixture was immediately plunged into liquid nitrogen and frozen and then lyophilized at −52 °C for 48 h (Alpha 1-2 LDplus, Martin Christ GmbH, Germany) until dry AuNP powder was obtained. In addition to the AuNP's, Zn dust was also used in ultrafine form through the grinding process.

Lactose Trituration of AuNP's and Zn Dust. Similar to the traditional homeopathic process wherein metal powders are triturated (intimately mixed by grinding) with lactose before serial dilutions, we triturated both AuNP's and Zn dust with lactose in a ratio of 1:5 in a mortar for 30 min. We chose a ratio of 1:5 (instead of 1:10 used in traditional manufacturing) to avoid masking the interactions in the presence of excess lactose.

Fourier Transform Infrared (FT-IR) Spectroscopy of Lactose-Triturated Mixtures. The IR spectra of plain lactose and the triturated mixtures were recorded on an FT-IR spectrometer (Perkin-Elmer-Spectrum One) in transmission mode using KBr discs, each with 20 repeating scans. KBr used in the experiment was oven dried followed by vacuum drying and subsequent storage in a glovebox before use. Each sample was vacuum dried and stored in an inert atmosphere of nitrogen prior to analysis. The results were plotted as wavenumber (cm^{-1}) against percentage (%) transmittance to compare the relevant frequency shifts due to the interaction of lactose on AuNP and Zn particle surfaces. The spectra were analyzed in the region of 4000−500 cm^{-1}. Some areas in the spectra were magnified with the scale bar intact for a better resolution of closely spaced peaks.

Transmission Electron Microscopy (TEM)/Selected Area Electron Diffraction (SAED) Analyses of Triturated Mixtures. The TEM and SAED analyses were performed on a JEM 2100 high-resolution TEM (JEOL, Japan). The triturated mixtures were dispersed in 90% v/v ethanol. After ensuring proper dispersion as seen by the lack of visible clumps in the suspension, the mixtures were filtered through 0.22 μm filters. The resulting clear dispersions were then sonicated for 5 min, and a drop of each was placed on TEM grids in a clean room to prevent artifacts. The grids were allowed to air dry for approximately 30−60 min, and then were placed under an IR lamp to ensure the complete removal of solvent molecules adhering to the particles. All samples were viewed at 200 kV.

Succussion, Sparging, and Ultrasonication Processes. For serial dilution experiments or high-speed videography, a 250 mL capacity borosilicate glass container was filled with 150 mL of 90% v/v ethanol with suspended AuNP's. In succussion, the container was subjected to vigorous manual pounding on a rubber sheet (20 times in 5 min with short intervals of a few seconds between strokes). In the serial dilution experiments, the samples were subjected to inductively coupled plasma-atomic emission spectroscopy (ICP-AES) or inductively coupled plasma-mass spectroscopy (ICP-MS), whereas in high-speed videography a single succussion stroke was given and the process was recorded. Because succussion yielded numerous bubbles on impact, we studied other similar processes such as sparging and ultrasonication that produced bubbles. For sparging, a sintered-glass sparger with micrometer-sized pores was used to pass air at a rate of 3 L/min for 5 min (the time required for 20 succussion strokes). For ultrasonication, a digital sonifier (Branson Ltd., USA) was operated at 20% amplitude with a frequency of 20 kHz for 5 min, with alternating sonic pulses of 5 s followed by a break of 2 s.

High-Speed Digital Videos of Succussion, Sparging, and Ultrasonication Processes: A Comparative Study. High-speed videos of the three processes were captured using the Phantom v12.1 (Vision Research Inc., USA) at a camera speed of 2000 fps with a resolution of 640 × 480 pixels. The videos were recorded by placing the camera at various heights so that the top and bottom of the liquid in the container could be filmed. In succussion, the camera was switched on immediately prior to the impact of the container on the elastic block and continued until the solution in the bottle became stationary after a highly turbulent phase immediately after impact. Similar videos were also taken for sparging and ultrasonication. The frames at the point of impact in succussion, initiation of bubble formation in sparging, and ultrasonication were taken as $t = 0$, and the time lapse of the subsequent frames was calculated accordingly. Representative snapshots of the three processes at various time intervals are presented.

Estimation of AuNP's in the Top Layer (TL) and Middle Layer (ML) of the Solution by ICP-AES and ICP-MS. AuNP concentrations were analyzed in the TL and the ML of the samples using ICP-AES and ICP-MS after serial dilutions with the three processes mentioned above.

AuNP powder (3 mg) was triturated either alone or with 1.5 g of lactose for 30 min in a mortar. The triturated AuNP's with or without lactose were then added to 150 mL of 90% v/v ethanol in a glass container maintaining a lactose/ethanol ratio of 1:100, thus mimicking the first centesimal (1:100) dilution in the homeopathic process after the initial solid triturations. The solutions were swirled to ensure thorough mixing of the contents. The containers were kept stationary for an hour, at the end of which 1.5 mL of TL and ML was removed (unprocessed samples) and an equivalent amount of solvent (3 mL) was replaced in the container. The bottle was then either succussed 20 times or sparged or ultrasonicated for 5 min depending upon the process and kept stationary for 45 min, after which 1.5 mL of TL and ML was removed. The TL sample was transferred to 148.5 mL of fresh 90% v/v ethanol in a new container, whereas the ML sample was analyzed directly. The procedure was followed for seven serial dilution steps. The Au concentrations were determined on an Ultima 2 ICP-AES instrument (Jobin Yvon Horiba, Japan; LOD 10 ng/mL).

Since the asymptotic region was far below the LOD of the ICP-AES instrument, an experiment with highly sensitive ICP-MS (Finnigan ELEMENT2, Thermo Electron Corporation, USA; LOD <1pg/mL) was performed. A procedure similar to that mentioned above was followed. Serial dilutions of up to 15c (final dilution factor of 10^{30}) were made by repeated succussion−dilution steps, and the AuNP concentrations were estimated.

dx.doi.org/10.1021/la303477s | Langmuir XXXX, XXX, XXX−XXX

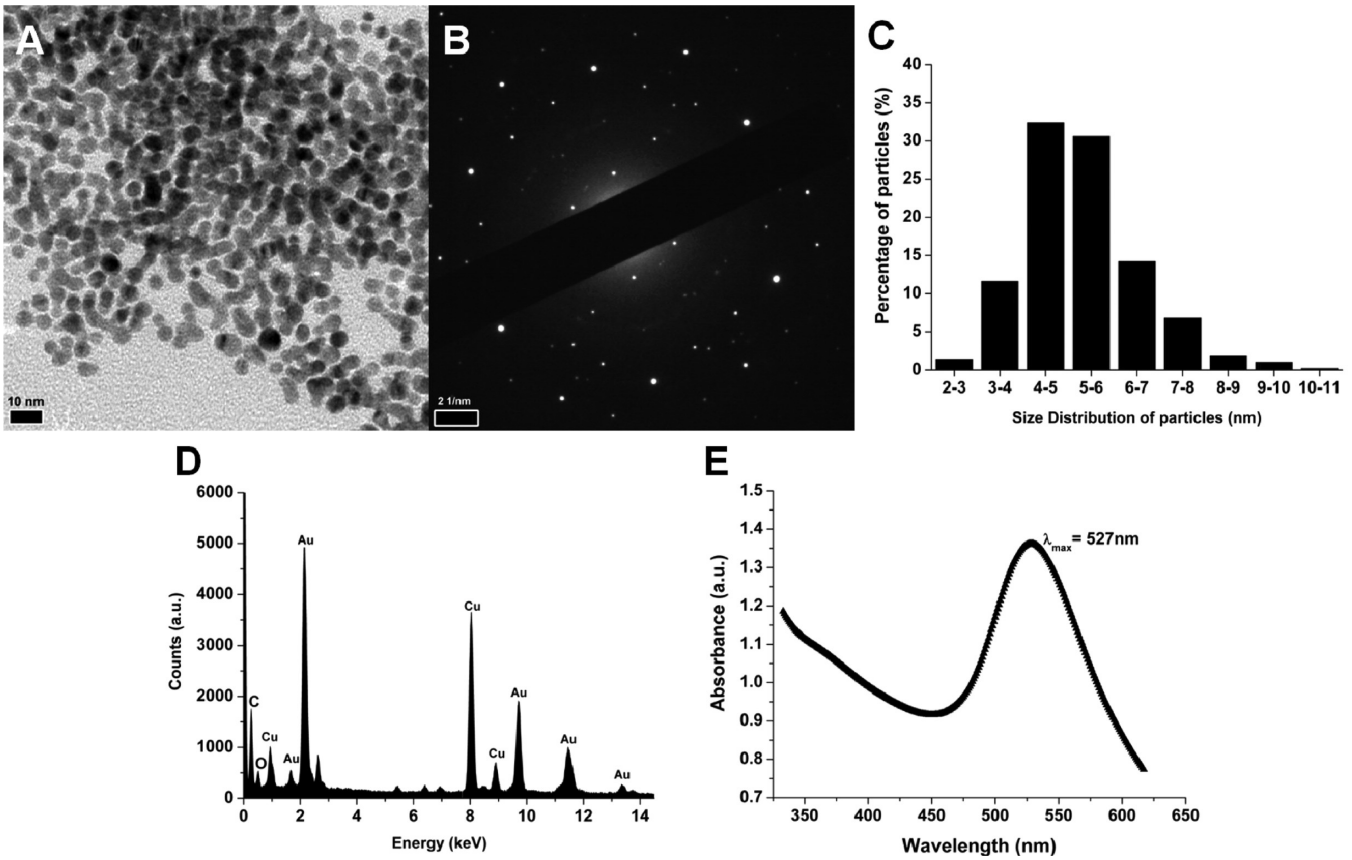

Figure 1. AuNP's synthesized for the hypothesis studies. (A) Bright-field TEM micrograph of AuNP's (scale bar = 10 nm). (B) SAED pattern of the particles. (C) Size distribution of the nanoparticles. (D) EDS spectrum of the AuNP's. Distinct peaks of Au are visible in the spectrum. (E) UV–visible spectroscopy data with a λ_{max} for AuNP's at 527 nm.

For estimating gold, a similar sample preparation method was used for both techniques. The samples were prepared by evaporating the ethanol to complete dryness in a vacuum rotary evaporator (Roteva model no. 8706R, Equitron, India) at 45 °C and 100 rpm. The residues were acidified with aqua regia, and the final volume of the sample was adjusted to 2 mL with Milli-Q water. The samples were filtered through Whatman 40 filter paper to remove any residual matter prior to analyses. The concentrations of AuNP's in the ML and bulk were directly obtained from ICP-MS or ICP-AES, whereas those in the TL were back-calculated (Supporting Information, Tables S1 and S2, respectively). For ICP-AES, an emission line of 242.795 nm was selected for measuring the concentration of gold, whereas in ICP-MS, gold concentrations were determined by a mass spectrometer. The instrument response was calibrated using standards prior to analyses of the samples.

RESULTS AND DISCUSSION

Synthesis of AuNP's. The AuNP's were synthesized according to the procedure described in the Methods section. Figure 1A illustrates the TEM bright-field image of the nanoparticles indicating the formation of spherical particles, with a narrow size distribution between 2 and 10 nm, with approximately 94% between 3 and 8 nm (Figure 1C). The *d*-spacing values obtained from the ED pattern of the particles (Figure 1B) confirm the formation of AuNP's. Additionally, the EDS and the UV–visible spectroscopic analyses (Figure 1D,E respectively) indicate Au in the spectrum and a λ_{max} peak at 527 nm, respectively, consistent with the formation of AuNP's.

For our studies, bare, uncoated AuNP powder that could be used in studies involving lactose trituration simulating the homeopathic manufacturing process was prepared. The particle-size range of the synthesized AuNP's harmonized with the crystallite sizes of 5–10 nm obtained in the dark-field TEM of the nanoparticles in the homeopathic solutions in our earlier studies.[9]

FT-IR Spectroscopy of Lactose-Triturated Mixtures. An FT-IR study was performed to examine any interaction of lactose with the raw material particles during trituration, the first step in homeopathic manufacturing. Figure 2A–C shows the IR spectra of plain lactose, AuNP–lactose and Zn dust–lactose triturated mixtures, respectively. Several characteristic features of chemical interactions between lactose and metal particles (gold and zinc) were observed in the spectra.

In plain lactose, two characteristic O–H stretching vibrations—secondary alcohol [$R_2CH(OH)$] at 3382 cm^{-1} and primary alcohol [RCH_2OH] at 3350 cm^{-1}—are observed in the spectra (Figure 2A).

Typically, for AuNP's prepared by the reduction of gold salt in the presence of water, the AuNP surface is reported to undergo partial hydroxylation, forming Au–OH (pK_a 3.2).[11] However, the dominant surface ion (–OH or $-O^-$) is dictated by the pK_a of the hydroxylated gold surface. When the pH of the surrounding medium is below the pK_a of the hydroxylated gold surface, then –OH groups are dominant, but if the pH is above the pK_a, then $-O^-$ groups prevail.[12]

In our case, the AuNP surface will be dominated by $-O^-$ ions,[13,14] which will tend to form hydrogen bonds with lactose through primary –OH or secondary –OH depending on the steric approach. Figure 2B depicts the most likely short-range interaction. We observed a distinct lowering of the mean

dx.doi.org/10.1021/la303477s | *Langmuir* XXXX, XXX, XXX–XXX

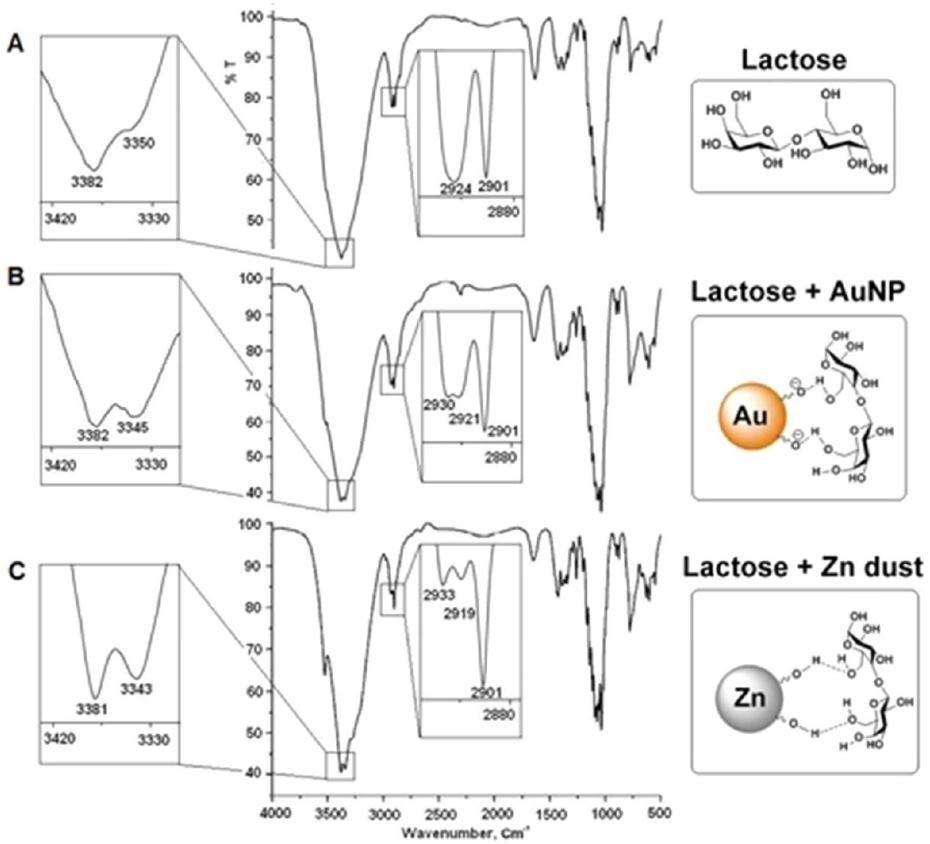

Figure 2. FT-IR spectra showing the lactose interactions with metal particles after trituration in a 1:5 ratio. (A) Plain lactose, (B) lactose + AuNP, and (C) lactose + Zn dust. The insets give (A) the structures of lactose and the bonding of lactose molecules with (B) AuNP's and (C) Zn dust. The AuNP−lactose bonding is through the H atom of the primary alcohol (CH_2−OH) group with the O^- ion on the AuNP surface. In the case of Zn−dust, the most favorable conformation is likely through the bonding of the H atom of the Zn surface hydroxyl group with the lone-pair electrons of the O atom of the primary alcohol group.

stretching frequency of −OH to 3345 cm^{-1} as compared to 3350 cm^{-1} in free lactose, indicating the presence of strong hydrogen bonding via sterically favored primary −OH.[15] A similar observation was made in the analysis of the triturated mixture of Zn dust with lactose (Figure 2C) with a mean stretching frequency of 3343 cm^{-1}, indicating hydrogen bonding through the primary O−H moiety.

Apart from the −OH frequency shifts, changes were also observed in the vibrational frequencies of methylene C−H bonds. In the case of plain lactose, two peaks at 2901 cm^{-1} and 2924 cm^{-1} corresponding to aliphatic methyne (R_2CH−) and methylene (RCH_2−) were obtained (Figure 2A).

In the AuNP−lactose triturated mixture, although the peak at 2901 cm^{-1} remains constant, the peak due to methylene (RCH_2−) is split into two separate peaks of equal intensities at 2930 cm^{-1} (antisymmetric stretch ν_{as}(C−H)) and 2921 cm^{-1} (symmetric stretch ν_s(C−H)) (Figure 2B). This is a clear indication of the effective interaction between lactose primary −OH and the AuNP surface.

Similar results were obtained in the case of the Zn dust−lactose triturated mixture, wherein the methylene (RCH_2−) peak was split into two peaks of equal intensities at 2933 cm^{-1} [ν_{as}(C−H)] and 2919 cm^{-1} [ν_s(C−H)] (Figure 2C). Zinc exists as ions with hydroxyl counterions at the surface, hence facilitating stable hydrogen bonding interactions. Whereas in AuNP−lactose the interaction of lactose with the Au−O^- surface is likely through the hydrogen atom of the primary alcohol, in the case of the Zn dust−lactose triturated mixture, the hydrogen atom on the partially hydroxylated zinc surface preferentially bonds through the lone pair electrons on the oxygen atom in lactose OH (Figure S1, Supporting Information).

From the spectra, it is evident that the lactose molecules stabilize the gold or zinc particles by noncovalent interactions in different ways. Although the predominant interaction is via the primary O−H in both the cases, a combined role of both primary and secondary O−H in lowering the mean frequency and peak broadening due to hydrogen bond formation cannot be ruled out. This interaction of lactose stabilizes the nanoparticle fraction generated during the trituration process, which is analogous to the top-down approach of nanoparticle formation resulting in the separation of the nanofraction from the coarser particles. To confirm the purported role of lactose as a stabilizer as obtained in the FT-IR results, TEM analyses of the triturated mixtures were carried out by dispersing them in 90% v/v ethanol.

TEM/SAED Studies of Lactose-Triturated Mixtures. TEM studies of AuNP−lactose triturated mixtures (figure 3A) demonstrate the formation of nanoclusters of AuNP's (dark areas in Figure 3A) embedded within a mesh of lactose (gray areas in Figure 3A). Figure 3B,C shows the SAED patterns of the dark (AuNP's) and gray (lactose) regions within the nanocluster, respectively. The SAED patterns clearly reveal the crystalline AuNP embedded within the amorphous lactose.

Similar observations of the formation of nanoclusters were made in trituration studies of lactose with zinc dust (325 mesh,

dx.doi.org/10.1021/la303477s | Langmuir XXXX, XXX, XXX−XXX

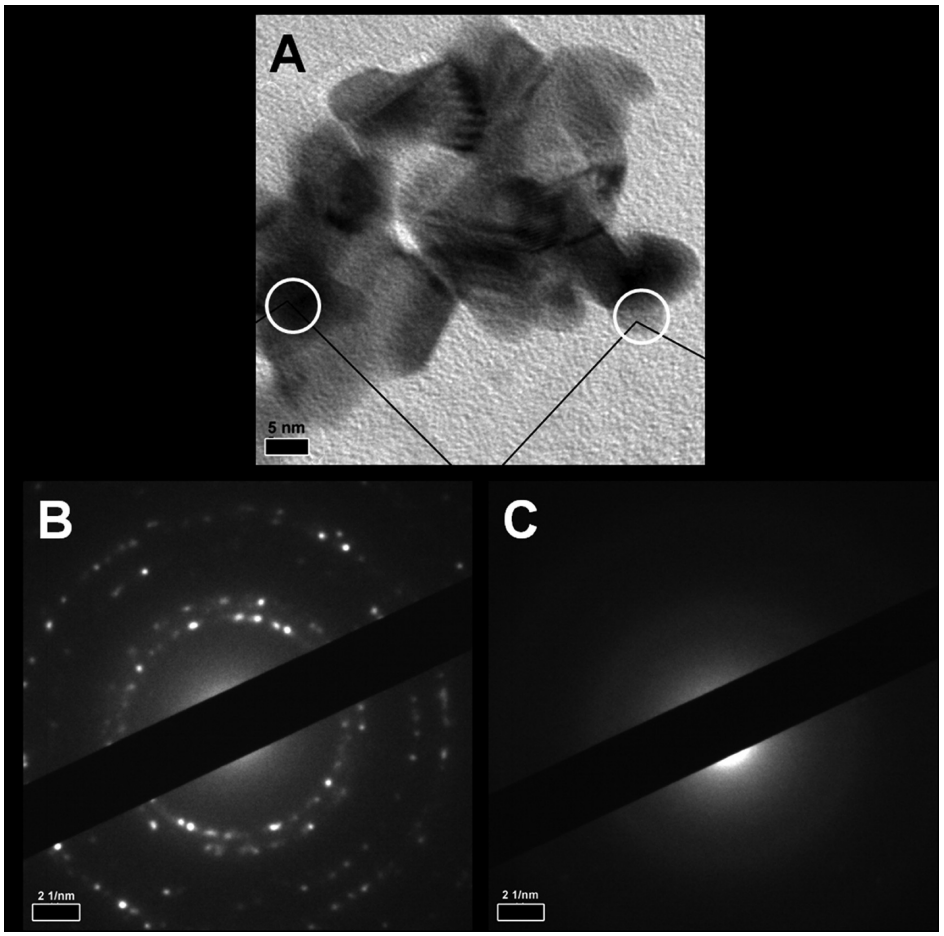

Figure 3. TEM analysis of a 1:5 AuNP−lactose triturated mixture. (A) Bright-field image of a lactose-embedded nanocluster of AuNP formed during trituration (scale bar = 5 nm). (B) SAED pattern of the AuNP embedded within the nanocluster showing a polycrystalline pattern consistent with the gold JCPDS data. (C) SAED pattern of the lactose in the nanocluster showing an amorphous pattern.

~44 μm particles). The zinc nanoclusters (not represented in the article) indicate the formation of 10−20 nm zinc nanoparticles. The formation of nanoparticles from the larger particles highlights the importance of the trituration process in the generation of the nanofraction.

In the manufacturing of synthetic nanoparticles, stabilizers or capping agents are routinely added to nanocolloids to coat the nanoparticle surface and prevent their aggregation. The generation of nanoclusters as evident from the TEM analyses clearly highlights a similar role of lactose as a stabilizer, akin to those used in synthetic processes. Lactose aids in preventing the aggregation of the nanometer-sized particles formed during the grinding process, thereby effectively segregating the nanofraction from the coarser particles in the subsequent dilution steps. ICP-AES and ICP-MS studies were used to ascertain whether the lactose-stabilized nanoparticles were retained better than the uncoated particles.

High-Speed Digital Video of the Succussion Process. The succussion process was studied in detail using high-speed videography. Representative snapshots of the video of the bottom and top surfaces of the liquid in the glass container have been presented in Figure 4A,B, respectively. In Figure 4B, at the point of impact of the container, a liquid whirlpool was clearly visible. This whirlpool, having started at the top of the liquid, reached the bottom, ensuring its complete swirling, thereby leading to the formation of flotation-sized air bubbles at the bottom as represented in Figure 4A.

These large entrapped air bubbles have the velocity to overcome various drag and gravitational forces in the liquid and rise to the air−liquid interface (Figure 4B). These rising air bubbles could be instrumental in levitating the nanoparticles from the bulk to the interface, forming a particle-enriched surface as explained in detail later. To verify our claim of air bubbles being the decisive factor in particle levitation, we performed ICP-AES and ICP-MS experiments to validate the enriched nanoparticle presence at the interface, possibly by the formation of a monolayer or a submonolayer on the liquid surface.

Similarly, we have demonstrated bubble formation during sparging (Figure S2A,B, Supporting Information) and ultrasonication (Figure S3A,B, Supporting Information).

A quantitative size determination of the bubbles (Figure 5) in the three processes revealed that in ultrasonication (Figure 5A), at the bottom, approximately 73% of the bubbles formed were smaller than 1 mm whereas the remaining were between 1 and 2 mm in diameter. On the contrary, at the air−liquid interface only about 28% were below 1 mm whereas approximately 50% were between 1 and 2 mm and approximately 21% were between 2 and 3 mm. This indicates an increase in the bubble size, which is expected as a result of bubble coalescence during levitation.

Succussion, however, showed almost monodisperse bubble formation with almost 74% in the size range of 1 to 2 mm and

dx.doi.org/10.1021/la303477s | *Langmuir* XXXX, XXX, XXX−XXX

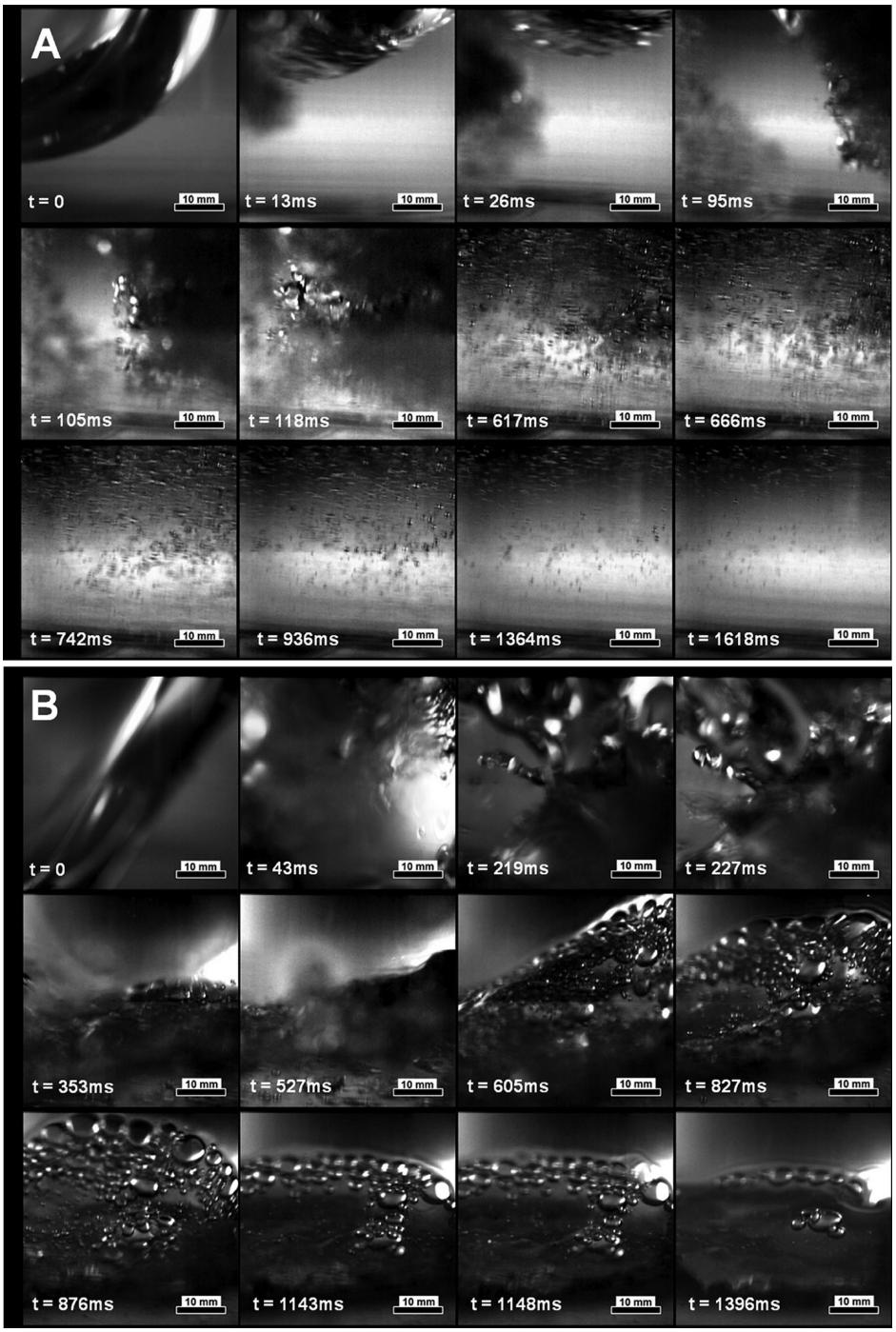

Figure 4. High-speed video images of the liquid in the container during succussion. The images represent a 4.5 cm × 4.5 cm area of the container. (A) Generation of air bubbles on the bottom. The hydrodynamic swirling of the liquid interface through the bulk liquid causing air entrapment is perceived. The swirling results in the formation of flotation-sized air bubbles at the bottom of the container. (B) Bubbles at the top of the liquid. The entrapped air bubbles generated at the bottom rise to the air−liquid interface. These flotation-sized air bubbles during succussion facilitate the levitation of the nanoparticles from the liquid bulk to the interface. The time from the point of impact has been given on the individual images (scale bar = 10 mm).

26% below 1 mm in diameter (Figure 5B) at the bottom with larger bubbles at the top, a trend similar to ultrasonication.

Unlike ultrasonication and succussion, in sparging (Figure 5C), large bubbles were observed. Approximately 8% were <1 mm, 45% were between 1 and 2 mm, and the remaining were larger than 2 mm, with a few even larger than 10 mm in diameter. In this case, however, a negligible variation in the size distribution was observed on the top surface.

We also used ICP-AES and ICP-MS to analyze whether these differences in bubble size were responsible for differential particle levitation in terms of the absolute concentrations at the interface.

Estimation of AuNP Concentrations in TL and ML by ICP-AES and ICP-MS. The ICP-AES and ICP-MS studies were performed to validate the TL surface enrichment of AuNP's with simultaneous depletion from the bulk and ML

dx.doi.org/10.1021/la303477s | *Langmuir* XXXX, XXX, XXX−XXX

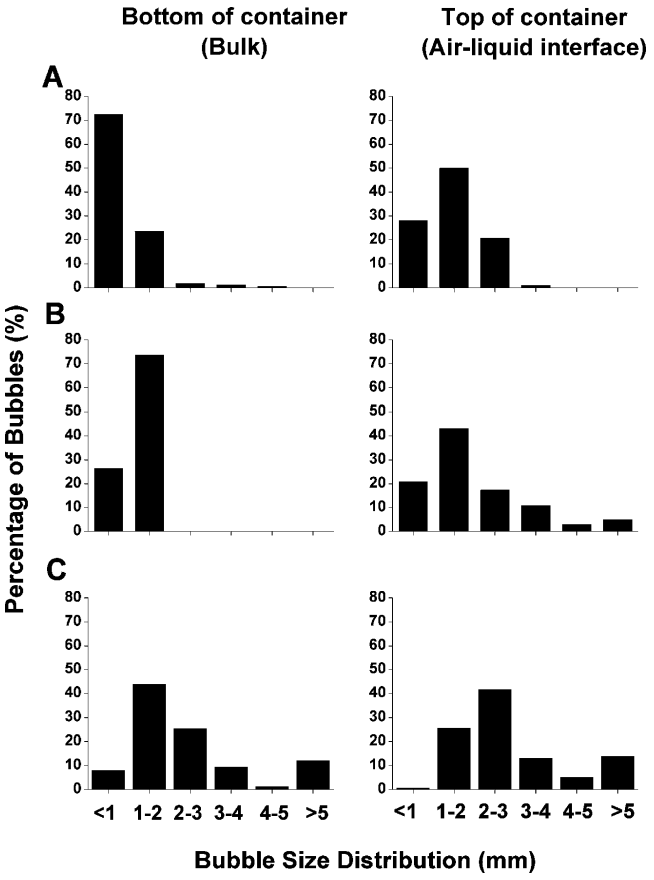

Figure 5. Size distribution of bubbles generated in (A) ultrasonication, (B) succussion, and (C) sparging. A progressive increase in the bubble sizes at the bottom is observed, where ultrasonication produces the smallest and sparging produces the largest size. In all three processes, an increase in bubble size at the interface is evident, as a result of bubble coalescence during levitation to the liquid surface.

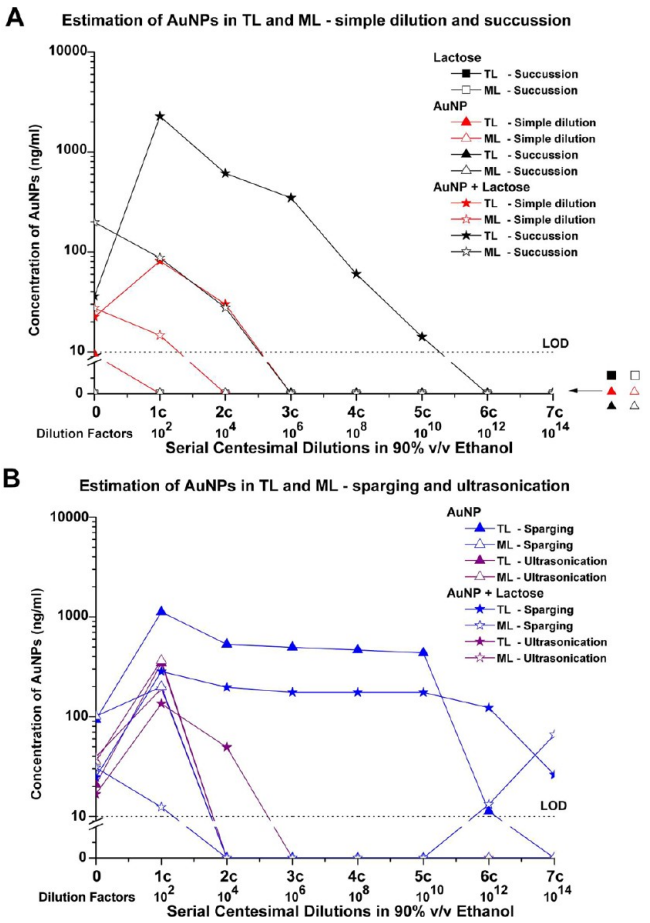

Figure 6. Estimation of AuNP concentrations in TL and ML by ICP-AES. 0 = unprocessed TL and ML samples and 1c−7c = serial 1:100 dilution steps. Estimated concentrations in (A) samples with simple dilutions and with succussion and (B) samples with sparging and ultrasonication. (Squares + black lines) plain lactose, (triangles) bare AuNP's, (stars) AuNP + lactose triturated mixture. (Open symbols) ML samples, (solid symbols) TL samples. (Red) Samples with simple dilution, (black) samples with succussion, (blue) samples with sparging, and (purple) samples with sonication. The dotted line at 10 ng/mL indicates the LOD of the instrument. Higher TL concentrations as compared to ML were observed. Also, the concentrations in succussed and sparged samples were higher than those for simple dilutions and ultrasonication, indicating the importance of the generation of bubbles and also their size and density.

after the three processes with or without lactose. The primary objectives of these studies were

(1) to study the effects of lactose trituration on the differential concentration of the nanoparticles between the bulk and the air−liquid interface and
(2) to study the effect of the size and density of generated air bubbles on the differential concentration of the nanoparticles between the bulk and the interface (i.e., the froth flotation of nanoparticles).

For this purpose, the differences in concentration between AuNP's in the TL and ML of the liquid were analyzed with (i) two types of nanoparticles (bare AuNP's and AuNP's triturated with lactose) and (ii) three methods of bubble formation (succussion, sparging, and ultrasonication). Two possible explanations with respect to our objectives in the experiments with the two types of nanoparticles and the three processes have been outlined below.

Effect of Lactose Trituration. In the dilutions of bare AuNP's with simple dilution, Au was not detected in the TL and ML samples (Figure 6A, solid and open red triangles, respectively). In the presence of lactose, however, the TL concentrations (solid red stars) were approximately 80 and 30 ng/mL in the first and second centesimal dilutions, respectively, and then below detection from the third dilution onward. The ML concentrations (open red stars) were much lower, at approximately 15 ng/mL for the first dilution and below the LOD from the second dilution (Figure 6A) onward.

When the process was repeated with succussion (Figure 6A), Au was not discerned in the TL and ML (solid and open black triangles, respectively) because of AuNP's settling as aggregates. On the contrary, in the succussed AuNP−lactose triturated mixture, measurable amounts of Au were detected in both layers (solid and open black stars for TL and ML, respectively), with the concentration in the TL being significantly greater than that in the ML. Although the ML concentrations fell below the LOD at the third centesimal (1:100 dilution), the TL concentrations reached the instrument's LOD only at the sixth dilution. There was a gradual decline in the TL concentrations from approximately 2500 ng/mL in the first dilution to about 15 ng/mL in the fifth dilution. The observed results are interesting because if the process had followed a logical serial

dx.doi.org/10.1021/la303477s | *Langmuir* XXXX, XXX, XXX−XXX

dilution then the concentrations in the TL should have diminished to below detection at the second dilution itself instead of the sixth, as was observed for the unsuccussed samples.

The above result is a clear demonstration of the bubble-induced flotation of nanoparticles arising from succussion (Figure 6A). We believe that succussion is analogous to traditional froth flotation techniques used in concentrating metals from ores, wherein metal-containing particles floated to the surface facilitated by froth or bubbles, as generated by the addition of frothing agents such as surfactants. In the succussion process, however, no surfactant is used, but it is clear from the video images that bubbles are indeed produced. We chose to study air sparging and ultrasonication further for their ability to generate bubbles and cause nanoparticle flotation.

In sparging (Figure 6B), high concentrations of Au were discerned in TL of the bare AuNP's and the AuNP−lactose triturated mixture. The Au concentrations in the bare AuNP's (solid blue triangles) reached approximately 1000 ng/mL in the first dilution and then formed a plateau at around 500 ng/mL until the fifth dilution, after which the concentration dropped below the limit of detection. Similarly, a plateauing effect at approximately 250 ng/mL in the TL of the triturated mixture (solid blue stars) was observed. The ML concentrations in both the cases (open blue triangles and open blue stars, respectively) were below the limit of detection in the second dilution (Figure 6B). A probable explanation of high concentrations in TL in the bare and triturated mixtures could be related to the extremely large sizes of the bubbles (larger than those in succussion) generated during sparging (Figure 5C) having the ability to levitate even small aggregates of AuNP's to the surface, which smaller bubbles in ultrasonication and succussion (Figure 5A,B) would not be able to do.

In ultrasonication, minute cavitation bubbles were formed, but very few reached the interface. This observation was corroborated in the Au concentrations discerned in the TL and ML of bare AuNP's and the AuNP−lactose mixture (Figure 6B). In bare AuNP's, TL (solid purple triangles) and ML (open purple triangles) concentrations were approximately 350 ng/mL at the first dilution but declined rapidly to below the LOD in subsequent dilutions. On similar grounds were the TL (solid purple stars) and ML (open purple stars) concentrations in the lactose-triturated mixture, which were approximately 150−200 ng/mL in the first dilution and then fell below the LOD from the third dilution onward (Figure 6B).

Effect of Bubble Size and Density. As discerned from the ICP-AES studies, the size and density of bubbles per unit area play vital roles in the particle levitation from the bulk. Apart from the density, the number of flotation-sized bubbles reaching the interface was found to be important. This is evident from Figure 6A,B, wherein both succussion and sparging with a higher density of flotation-sized bubbles exhibited higher TL concentrations as compared to ultrasonication exhibiting a sparse bubble population at the interface.

A significant bubble-size-dependent concentration gradient at the TL was observed especially for bare AuNP's, wherein large sparging bubbles were able to levitate small aggregates of nanoparticles, which the smaller succussion and ultrasonication bubbles were unable to do.

The overall results from ICP-AES suggest higher TL concentrations as compared to those for ML, which are strongly dependent on the initial presence of lactose as a nanoparticle stabilizer and the extent of froth generated.

We believe that the actual asymptotic region commenced at these extremely low concentrations. To validate our theory of asymptote formation, the study of a AuNP−lactose triturated mixture with succussion as a source of froth generation was carried out with ICP-MS (Figure 7).

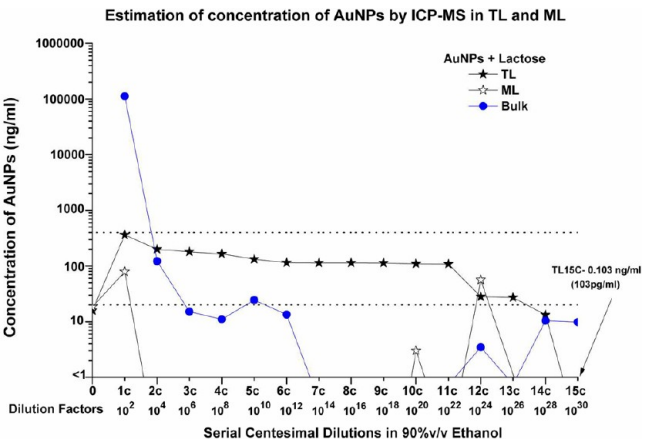

Figure 7. Estimation of AuNP concentrations in TL and ML after succussion by ICP-MS. Validation of asymptote formation. 0 = unsuccussed TL and ML samples and 1c−15c = serial 1:100 dilution steps. Asymptote formation is observed at the TL (solid black stars) concentrations. The TL concentrations plateaued between a 20-fold range of 20−400 ng/mL, which is negligible in comparison to 14 centesimal dilutions (dilution factor of 10^{28}). In the asymptotic curve beyond 6c, <1% of the total Au is retained and the rest is transferred to the next dilution. The asymptotic curve indicates a bubble-induced froth flotation process of nanoparticles forming a monolayer at the air−liquid interface.

As evident from the graph, the TL concentrations of Au formed a plateau in a narrow 20-fold concentration range between 20−400 ng/mL over 14 centesimal dilutions (dilution factor of 10^{28}) and then decreased to a concentration of 0.103 ng/mL at the 15th dilution. The concentrations measured in the bulk and in the ML (the concentration retained in the previous dilution and not carried forward) decreased with increasing dilution, and beyond 6c dilution, <1% of the total concentration of Au (Table 1) remained, indicating that almost the entire quantity of Au particulate matter levitated to the top of the liquid and was transferred to the subsequent dilution. However, a few variations were observed in the retained concentrations from 12c to 15c, pointing toward the extreme sensitivity of the method in which the dilutions are actually carried out.

In the actual homeopathic manufacturing process, only 1% of the previous dilution is transferred to the next dilution step. In our experiments, the height of the liquid in the container was approximately 6 cm, meaning that the monolayer of particles from the 1% of liquid volume would be only the top 0.6 mm of the liquid surface. The difficulty in skimming off this top 1% manually and transferring to the next dilution was evident from the sudden drop in the TL concentrations at certain dilutions, illustrating the extreme sensitivity of these processes. Such extreme sensitivity could be responsible for the enormous variations in starting metal concentrations and asymptote formation at different concentration levels between batches of

dx.doi.org/10.1021/la303477s | *Langmuir* XXXX, XXX, XXX−XXX

Table 1. Validation of Asymptote Formation: Actual Measured AuNP Concentrations in ML, the Bulk, and TL after Succussion by ICP-MS[a]

dilution	ML (ng/mL)	bulk (B) (ng/mL)	TL (ng/mL)	amount retained in previous dilution (%)	amount transferred to next dilution (%)
0	18.413	not analyzed	15.870		
1c	78.684	112 328.246	**361.824**	44.80	
2c	0.047	121.539	**199.709**	10.12	55.20
3c	0	15.158	**179.498**	8.21	89.88
4c	0	11.057	**164.755**	19.83	91.79
5c	0	24.505	**132.082**	13.53	80.17
6c	0	13.410	**114.202**	0.44	86.47
7c	0	0.378	**113.698**	0	99.56
8c	0	0	**113.698**	0.58	100.00
9c	0	0.467	**113.075**	3.55	99.42
10c	3.013	0	**109.058**	0.96	96.45
11c	0.05	0.734	**108.013**	73.92	99.04
12c	56.415	3.469	**28.168**	3.54	26.08
13c	0	0.748	**27.171**	51.20	96.46
14c	0	10.433	**13.260**	99.22	48.80
15c	0	9.842	0.103		0.78

[a]0, unsuccussed ML and TL samples; 1c−15c, serial 1:100 dilution steps. The concentrations for all ML samples (ML0−ML15c), the bulk (B1c−B15c), and TL (TL0 and TL15c) were directly analyzed. The values in bold for TL1c−TL14c were back-calculated concentrations (detailed calculation in Table S2 in the Supporting Information). Beyond 6c, <1% of the AuNP is retained and the rest is transferred to the subsequent dilution. The high variation in the percentages of AuNP's retained and transferred beyond dilution 12c highlights the sensitivity of the manual process followed in homeopathic manufacturing. This variation corroborates the enormous interbatch variations of starting metals obtained in our earlier physicochemical studies.[9]

medicine of the same potency and manufacturer as observed in our physicochemical studies.[9]

In spite of the variations, the ICP-AES and ICP-MS experiments have underlined the formation of an asymptote and also highlighted the importance of various processes employed in the manufacturing of these extreme dilutions. On the basis of the results obtained from our experiments, we postulate a hypothesis of how extreme dilutions reach an asymptotic state.

Hypothesis of Surface Monolayer Formation and Retention. On the basis of the results above, we hypothesize a mechanism of nanoparticle formation and retention, illustrated in Figure 8, wherein the first step (A) generates nanoparticles from the raw material by the process of grinding or comminution. The lactose caps the particles during grinding, whereas bubbles generated in subsequent succussions enable the flotation of the nanoparticles to the surface. Serial dilution, which follows, is done by transferring the surface layer, now enriched with nanoparticles, to the next stage of dilution. This is repeated for every step; therefore, the concentration of nanoparticles does not drop below a threshold that is determined by the surface concentration.

Step A: Solid Trituration with Lactose. During the manufacturing of these extreme dilutions, the raw materials are first triturated with lactose until the 6x potency is reached (where 'x' indicates decimal dilution with a ratio of 1:9 of raw material/lactose). The first grinding step at potency 1x is deemed to be complete only when approximately 80% of the particle sizes of the starting raw material are below 10 μm and none are above 50 μm in size.[16]

Our trituration studies highlight the importance of grinding in nanofraction formation, with lactose playing the indispensible role of a stabilizer, effectively separating the generated nanoparticles from the larger bulk raw material. Lactose also prevents the aggregation of these nanoscale particles by nanocluster formation made up of a few raw material nanoparticles embedded in a mesh of lactose (Figure 3).

The pulverization also generates extreme pressures resulting in a rough nanoparticle surface that can effectively entrap air within the crevices and play a significant role in the ensuing stages. This process is similar to the top-down approach of the synthesis of nanoparticles.

Step B: Ethanolic Dispersion. After the solid trituration, in the serial ethanolic dilutions, the larger raw material particles settle in the container whereas the nanoclusters are dispersed freely in the medium. The entrapped air within the crevices on the surface of the particles would still persist. Gas supersaturation is initiated at this stage within the crevices on the particle surface, resulting in the formation of surface nanobubbles.

Steps C and D: Succussion and Surface Turbulence. During succussion, the surface turbulence as a result of the pounding initiates various key mechanisms responsible for the final particle retention.

Mechanism 1: Formation of Nanobubbles Due to Gas Supersaturation. In addition to the nanobubbles of entrapped air during the liquid dispersion, the liquid turbulence at impact creates intense pressures resulting in a higher solubility of gases in the solvent. The increased amount of dissolved gases facilitates supersaturation within the surface crevices, resulting in nanobubble formation at the solid−liquid interface. Once these nanobubbles frost the nanoparticle surface, they readily cling to the surface because of their lower ascending velocity and high surface free energies. Studies on nanobubbles have shown that they have very long lives,[17] at least for a few hours. The nanobubbles were also found to be very stable because the pressures inside them were estimated to be equal to the pressure of the surrounding liquid.[18−23]

Mechanism 2: Air Bubble Formation Due to Air Entrapment. The extreme turbulence also effectively entraps air from the container headspace (Figure 4A,B). The liquid vortex formed at the surface reaches the bottom of the container, ensuring thorough mixing of the contents. These flotation-sized entrapped air bubbles rising to the liquid surface are responsible for the particle retention through subsequent dilutions.

Steps E and F: Formation of the Nanoparticle−Bubble Complex and Levitation to the Liquid Surface. Here, both mechanisms converge. Although the surface nanobubbles by themselves are unable to levitate the particles to the surface because of their extremely small sizes, the large air bubbles alone cannot directly attach to the hydrophobic particle surfaces. In the absence of nanobubbles, the formed complex has a very small contact angle with low adhesion energy. This complex is easily disrupted during its ascent as a result of drag forces, gravitational forces, and the enormous hydrostatic pressure, resulting in particles remaining in the liquid bulk. The nanobubbles play a critical role at this point in facilitating the nanoparticle attachment to the air bubbles with a larger contact angle, augmenting the adhesion forces. The complex thus

dx.doi.org/10.1021/la303477s | Langmuir XXXX, XXX, XXX−XXX

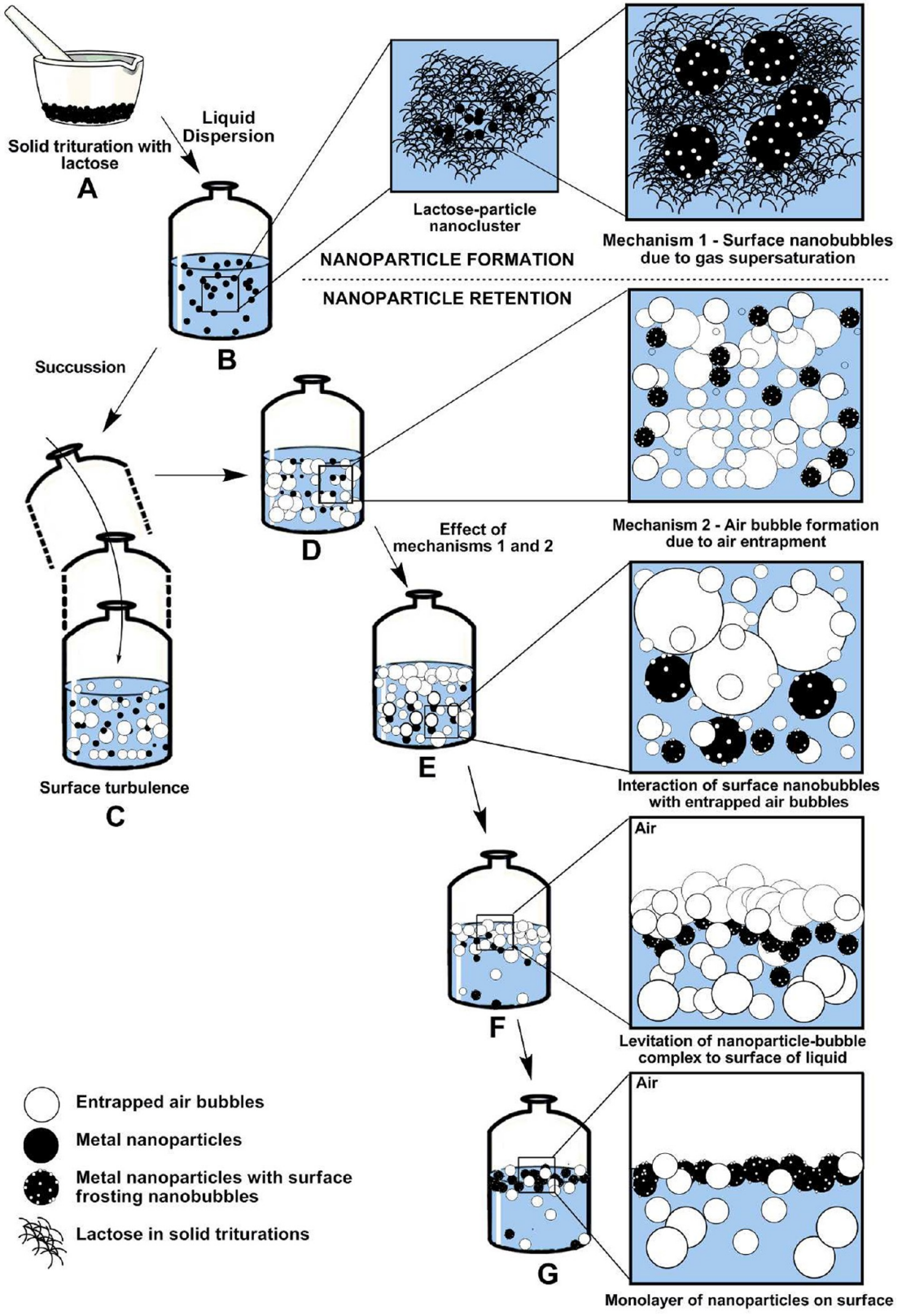

Figure 8. Stepwise representation of the surface monolayer hypothesis of particle retention. (A) The starting raw material is ground with lactose in a mortar. (B) The triturated mixture is dispersed in the solvent. (C) The container is then vigorously pounded (succussed) on a rubber stop. (D) Succussion results in surface turbulence generating air bubbles in the bulk. (E) The air bubbles attach the nanoparticles through the surface frosting nanobubbles. (F) The increased adhesion force allows the complex to rise to the liquid surface. (G) At the interface, the bubbles implode, but the particles remain on the surface, forming a monolayer that is retained through serial dilutions. For representation purposes, hence the bubbles and nanoparticles are not drawn to scale.

dx.doi.org/10.1021/la303477s | *Langmuir* XXXX, XXX, XXX–XXX

formed can easily rise to the liquid surface without disrupting.[24−26]

Step G: Monolayer of Particles on the Surface. Upon levitating to the surface, the larger air bubbles implode instantly. However, the particles having reached the air−liquid interface do not settle or disperse immediately into the liquid and remain as a monolayer. The above mechanism repeats at each dilution−succussion step, resulting in the effective formation and retention of this particle monolayer through serial dilutions.

CONCLUSIONS

On the basis of the results from our experiments, we have unequivocally shown that nanoparticles can be concentrated on the liquid surface in a manner similar to the traditional froth-flotation process used in the metal ore purification of larger particles. We have demonstrated that lactose during grinding helped in the formation of nanoclusters, whereas the ensuing processes such as succussion and sparging producing numerous large air bubbles aided nanoparticle levitation to the liquid surface, forming a monolayer that was preserved in the serial dilutions. We have shown that once the concentration of the AuNP's reached a threshold of a few ng/mL, further serial dilutions did not result in a concentration reduction and an asymptote was formed.

The validated surface monolayer hypothesis that we have proposed in this article could facilitate our understanding of these extreme dilutions, especially those used as homeopathic medicines, and could also help in explaining the presence of a finite amount of nanoparticles of the starting materials in commercial 30c and 200c metal-based homeopathic potencies.

ASSOCIATED CONTENT

Supporting Information

The most likely hydrogen-bonded lactose interactions with gold and lead nanoparticles. Representative images of a high-speed video of sparging demonstrating the large flotation-sized bubbles forming at the bottom and rising to the air−liquid interface. Sparse bubble generation at the bottom and very few reaching the air−liquid interface in ultrasonication. Detailed experimental schemes of ICP-AES and ICP-MS analyses for determining the ML/bulk concentrations. Formulas for back-calculating the TL concentrations. This material is available free of charge via the Internet at http://pubs.acs.org.

AUTHOR INFORMATION

Corresponding Author

*E-mail: sgkane@gmail.com, jb@iitb.ac.in.

Notes

The authors declare no competing financial interests.

ACKNOWLEDGMENTS

This work was supported primarily by a grant from S. Kane. Support in part came from the Narotam Sekhsaria Foundation and Mr. and Mrs. K. Patel. We gratefully acknowledge them and also thank the Department of Science and Technology (DST), Government of India, for support through FIST, Nanomission, IRPHA, SERC, and Indo-Spain schemes and for access to central and departmental facilities in the Centre for Research in Nanotechnology and Science (CRNTS) and Chemical Engineering, IIT Bombay.

REFERENCES

(1) Davenas, E.; Beauvais, F.; Amara, J.; Oberbaum, M.; Robinzon, B.; Miadonna, A.; Tedeschi, A.; Pomeranz, B.; Fortner, P.; Belon, P.; Sainte-Laudy, J.; Poitevin, B.; Benveniste, J. Human Basophil Degranulation Triggered by Very Dilute Antiserum Against IgE. *Nature* **1988**, *333*, 816−818.

(2) Chaplin, M. F. The Memory of Water: An Overview. *Homeopathy* **2007**, *96*, 143−150.

(3) Teixeira, J. Can Water Possibly Have a Memory? A Sceptical View. *Homeopathy* **2007**, *96*, 158−162.

(4) Rao, M. L.; Roy, R.; Bell, I. R.; Hoover, R. The Defining Role of Structure (Including Epitaxy) in the Plausibility of Homeopathy. *Homeopathy* **2007**, *96*, 175−182.

(5) Anagnostatos, G. S. Small Water Clusters (Clathrates) in the Homoeopathic Preparation Process. In *Ultra High Dilution − Physiology and Physics*; Endler, P. C., Schulte, J., Eds.; Kluwer Academic Publishers: Dordrecht, The Netherlands, 1994; pp 121−128.

(6) Walach, H.; Jonas, W. B.; Ives, J.; van Wijk, R.; Weingärtner, O. Research on Homeopathy: State of the Art. *J. Altern. Complement. Med.* **2005**, *11*, 813−829.

(7) Davydov, A. S. Energy and Electron Transport in Biological Systems. In *Bioelectrodynamics and Biocommunication*; Ho, M. W., Popp, F. A., Warnke, U., Eds.; World Scientific Publishing Co. Pte. Ltd: Singapore, 1994; Chap. 17, pp 411−430.

(8) Anick, D. J.; Ives, J. A. The Silica Hypothesis for Homeopathy: Physical Chemistry. *Homeopathy* **2007**, *96*, 189−195.

(9) Chikramane, P. S.; Suresh, A. K.; Bellare, J. R.; Kane, S. G. Extreme Homeopathic Dilutions Retain Starting Materials: A Nanoparticulate Perspective. *Homeopathy* **2010**, *99*, 231−242.

(10) Martin, M. N.; Basham, J. I.; Chando, P.; Eah, S. K. Charged Gold Nanoparticles in Non-Polar Solvents: 10-min Synthesis and 2D Self-Assembly. *Langmuir* **2010**, *26*, 7410−7417.

(11) Sylvestre, J. P.; Kabashin, A. V.; Sacher, E.; Meunier, M.; Luong, J. H. T. Stabilization and Size Control of Gold Nanoparticles During Laser Ablation in Aqueous Cyclodextrins. *J. Am. Chem. Soc.* **2004**, *126*, 7176−7177.

(12) Male, K. B.; Li, J.; Bun, C. C.; Ng, S. C.; Luong, J. H. T. Synthesis and Stability of Fluorescent Gold Nanoparticles by Sodium Borohydride in the Presence of Mono-6-deoxy-6-pyridinium-β-Cyclodextrin Chloride. *J. Phys. Chem. C* **2008**, *112*, 443−451.

(13) Shi, H.; Stampfl, C. First-Principles Investigations of the Structure and Stability of Oxygen Adsorption and Surface Oxide Formation at Au(111). *Phys. Rev. B: Condens. Matter Mater. Phys.* **2007**, *76*, 075327-1 − 075327-14.

(14) Baker, T. A.; Friend, C. M.; Kaxiras, E. Atomic Oxygen Adsorption on Au(111) Surfaces with Defects. *J. Phys. Chem. C* **2009**, *113*, 3232−3238.

(15) Coates, J. Interpretation of Infrared Spectra: A Practical Approach. In *Encyclopedia of Analytical Chemistry*; Meyers, R. A., Ed.; John Wiley and Sons: Chichester, 2000; pp 10815−10837.

(16) Varma, P. N.; Vaid, I. In *Encyclopedia of Homoeopathic Pharmacopoeia & Drug Index*; B. Jain Publishers: New Delhi, 2007; pp 2722−2745.

(17) Seddon, J. R. T.; Zandvliet, H. J. W.; Lohse, D. Knudsen Gas Provides Nanobubble Stability. *Phys. Rev. Lett.* **2011**, *107*, 116101 -1−116101-4.

(18) Yang, J.; Duan, J.; Fornasiero, D.; Ralston, J. Very Small Bubble Formation at the Solid-Water Interface. *J. Phys. Chem. B* **2003**, *107*, 6139−6147.

(19) Zhang, X. H.; Khan, A.; Ducker, W. A. A Nanoscale Gas State. *Phys. Rev. Lett.* **2007**, *98*, 136101−1 − 136101−4.

(20) Tao, Y.; Liu, J.; Yu, S.; Tao, D. Picobubble Enhanced Fine Coal Flotation. *Sep. Sci. Technol.* **2006**, *41*, 3597−3607.

(21) Attard, P. Nanobubbles and the Hydrophobic Attraction. *Adv. Colloid Interface Sci.* **2003**, *104*, 75−91.

(22) Tyrrell, J. W. G.; Attard, P. Images of Nanobubbles on Hydrophobic Surfaces and Their Interactions. *Phys. Rev. Lett.* **2001**, *87*, 176104-1−176104-4.

(23) Zhang, X. E.; Maeda, N.; Craig, V. S. J. Physical Properties of Nanobubbles on Hydrophobic Surfaces in Water and Aqueous Solutions. *Langmuir* **2006**, *22*, 5025−5035.
(24) Zhou, Z. A.; Xu, Z.; Finch, J. A. On the Role of Cavitation in Particle Collection in Flotation − A Critical Review. *Miner. Eng.* **1994**, *7*, 1073−1084.
(25) Zhou, Z. A.; Xu, Z.; Finch, J. A.; Masliyah, J. H.; Chow, R. S. On the Role of Cavitation in Particle Collection in Flotation − A Critical Review II. *Miner. Eng.* **2009**, *22*, 419−433.
(26) Maoming, M.; Tao, T.; Rick, H.; Zhenfu, L. Nanobubble Generation and its Application in Froth Flotation (Part I): Nanobubble Generation and its Effects on Properties of Microbubble and Millimetre Scale Bubble Solutions. *Mining Sci. Tech.* **2010**, *20*, 0001−0019.